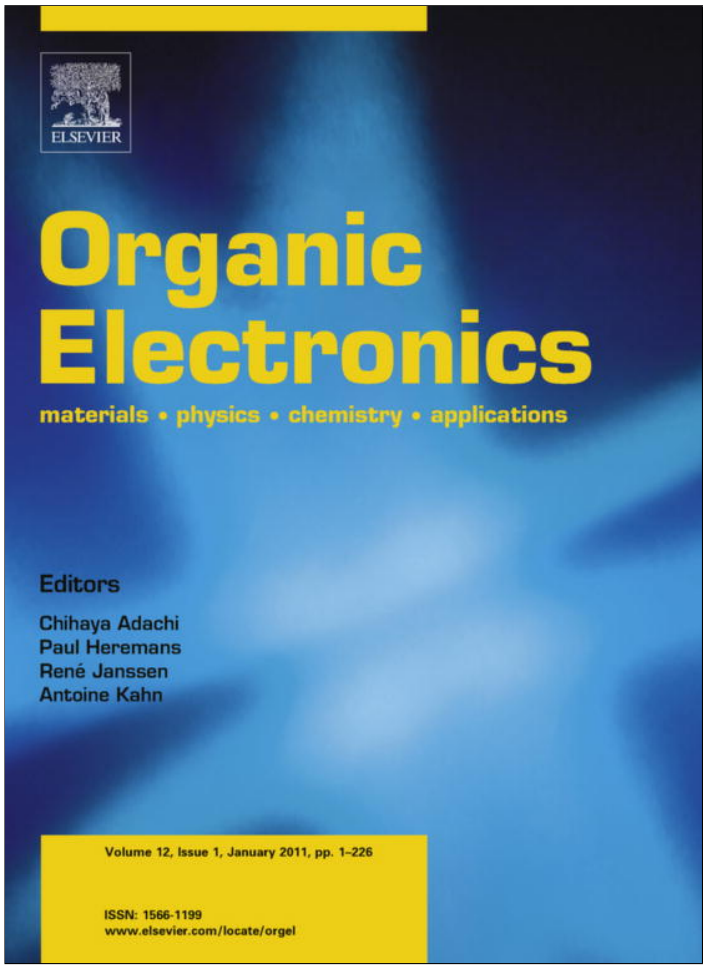

(This is a sample cover image for this issue. The actual cover is not yet available at this time.)

Organic Electronics 12 (2011) 1539–1543

Contents lists available at ScienceDirect

Organic Electronics

journal homepage: www.elsevier.com/locate/orgel

Letter

Inverted organic solar cells using a solution processed aluminum-doped zinc oxide buffer layer

Tobias Stubhan [a,*], Hyunchul Oh [a], Luigi Pinna [a,b], Johannes Krantz [a], Ivan Litzov [a], Christoph J. Brabec [a,b]

[a] Institute of Materials for Electronics and Energy Technology (I-MEET), Friedrich-Alexander-University of Erlangen-Nuremberg, Martensstraße 7, 91058 Erlangen, Germany
[b] Bavarian Center for Applied Energy Research (ZAE Bayern), Am Weichselgarten 7, 91058 Erlangen, Germany

ARTICLE INFO

Article history:
Received 16 December 2010
Received in revised form 23 May 2011
Accepted 29 May 2011
Available online 15 June 2011

Keywords:
Polymer solar cell
Solution processing
Inverted structure
Zinc oxide nanoparticles
Al doped ZnO
Electron injection layer

ABSTRACT

In this article, we demonstrate a route to solve one of the big challenges in the large scale printing process of organic solar cells, which is the reliable deposition of very thin layers. Especially materials for electron (EIL) and hole injection layers (HIL) (except poly(3,4-ethylene dioxythiophene):(polystyrene sulfonic acid) (PEDOT:PSS)) have a low conductivity and therefore require thin films with only a few tens of nanometers thickness to keep the serial resistance under control. To overcome this limitation, we investigated inverted polymer solar cells with an active layer comprising a blend of poly(3-hexylthiophene) (P3HT) and [6,6]-phenyl-C_{61}-butyric acid methyl ester (PCBM) with solution processed aluminum-doped zinc oxide (AZO) EIL. Devices with AZO and intrinsic zinc oxide (i-ZnO) EIL show comparable efficiency at low layer thicknesses of around 30 nm. The conductivity of the doped zinc oxide is found to be three orders of magnitude higher than for the i-ZnO reference. Therefore the buffer layer thickness can be enhanced significantly to more than 100 nm without hampering the solar cell performance, while devices with 100 nm i-ZnO films already suffer from increased series resistance and reduced efficiency.

1. Introduction

Polymer solar cells (PSCs) based on blends of conjugated polymers and fullerenes offer a promising alternative for the development of a low-cost and flexible photovoltaic technology [1,2]. Significant progress has been made in the performance of organic solar cells. For commercialization, large area production issues need to be solved and device reliability and lifetime need to be improved.

The polymer solar cells investigated in this work were fabricated according to the layer stack shown in Fig. 1, which is the so-called inverted architecture. This layer sequence offers advantages in stability compared to the normal device layout [3,4]. The necessity to use highly reactive and unstable low work function metals (e.g. Ca, Ba) to form an efficient contact for electron extraction is avoided in the inverted architecture [5] and stable high work function metals (e.g. Ag), which are also compatible to printing processes, can be employed to form a non-transparent top contact [6]. Additionally, the frequently used, but chemically unstable interface between poly(3,4-ethylene dioxythiophene):(polystyrene sulfonic acid) (PEDOT:PSS) and the indium-tin-oxide (ITO) anode is avoided [7].

ITO itself (WF: 4.75 eV) is a rather bad choice for the cathode material. It forms a non-selective interface to PCBM (4.3 eV), which results in surface recombination. The selectivity of the cathode is typically improved by

* Corresponding author. Tel.: +49 (0) 9131 852 7634; fax: +49 (0) 9131 852 8495.
E-mail addresses: tobias.stubhan@ww.uni-erlangen.de (T. Stubhan), oh@mf.mpg.de (H. Oh), luigi.pinna@ww.uni-erlangen.de (L. Pinna), johannes.krantz@ww.uni-erlangen.de (J. Krantz), ivan.litzov@ww.uni-erlangen.de (I. Litzov), christoph.brabec@ww.uni-erlangen.de (C.J. Brabec).

1566-1199/$ - see front matter © 2011 Elsevier B.V. All rights reserved.
doi:10.1016/j.orgel.2011.05.027

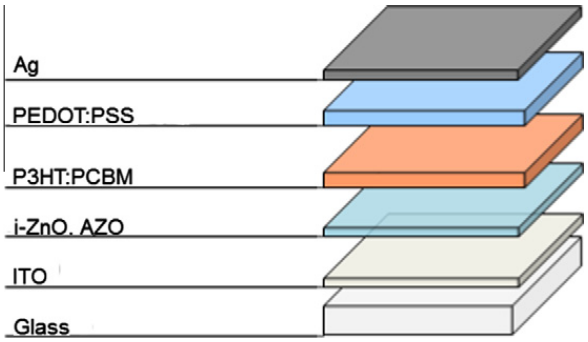

Fig. 1. Layer stack of the investigated solar cells.

using a metal oxide buffer layer between ITO and the semiconductor. One of the most intensely studied materials for this function is solution processed zinc oxide [3,8,9]. The energy levels of ZnO fit very well to the requirements for an electron injection layer. The work function is well matched to the PCBM lowest unoccupied molecular orbital (LUMO) and the valence band is deep below the highest occupied molecular orbital (HOMO) of most conjugated π-systems [10]. The wide bandgap of ZnO ensures high transmittance in the relevant spectral regime [11].

One of the few disadvantages of intrinsic ZnO (i-ZnO) is the restriction to a rather low film thickness of a few tens of nanometers due to the very low conductivity. Such a thin film imposes a major challenge for the manufacturing of polymer solar cells by high volume printing processes. On the one hand, complete coverage and a low density of pin-holes are challenging to achieve with thin film coatings. On the other hand, thin films may be less robust against mechanical stress being incurred during the subsequent printing processes. Such a robust electron injection layer is specifically important for the new generation of high performing semiconductors, which typically show the best efficiency with an active layer thickness of around or below 100 nm [12–17]. This concept is further applicable to multi-junction solar cells, where a reliable interface layer is essential to protect the lower half-cell [18].

In conclusion, we propose that thick interface layers are beneficial for enhanced device stability and increased production yield. The most straightforward way to enable thicker ZnO buffer layers is a conductivity increase via doping [11]. We are investigating aluminum (Al) as a dopant, because it is very cheap, non-toxic and resources are not limited. Vacuum processed aluminum-doped ZnO electrodes are used for various solar cell technologies like a-Si [19] or CIGS [20], and recently were also reported for organic solar cells [21].

In this work, we compare i-ZnO versus AZO, both processed from solution, as electron injection layers for organic solar cells. A dispersion of i-ZnO nanoparticles and an AZO precursor solution were prepared in organic solvents. The thin film properties of the two interface materials were characterized and the impact of their EIL thickness on the performance of the solar cells was compared. Overall, we found comparable device performance for thin i-ZnO and AZO layers. Increasing the EIL to ~100 nm results in significant performance loss in case of the i-ZnO, while cells with an AZO layer maintained their performance.

2. Materials and methods

The i-ZnO nanoparticles were prepared in methanol via hydroxylation of zinc acetate dihydrate ($ZnAc{\cdot}2H_2O$) by potassium hydroxide (KOH) adopting a method described by Harnack et al. [22] and afterwards dissolved in acetone at a concentration of 2 wt.%. The AZO solution was synthesized adopting a route described by Alam and Cameron [23] starting with a mixture of zinc acetate ($ZnAc{\cdot}2H_2O$) and aluminum hydroxide acetate ($HOAl(C_2H_3O_2)_2$) at a ratio of 1 at.%. Monoethanolamine (MEA) was added to the suspension to stabilize the Al doped ZnO complex.

The inverted photovoltaic devices were processed and characterized in ambient atmosphere. Pre-structured ITO coated glass substrates (as obtained from Osram) were subsequently cleaned in acetone and isopropyl alcohol for 10 min each. After drying, the substrates were coated with the organic precursor for AZO, respectively the i-ZnO solution, via doctor blading. Conversion of the precursor to AZO via hydrolysis was achieved by heating the samples to 260 °C for 10 min, while the i-ZnO film was dried at 150 °C for 10 min. Higher layer thicknesses were achieved via subsequent deposition steps. In case of AZO a calcination step was applied after each deposition. P3HT purchased from Merck and technical grade PCBM from Solenne were separately dissolved in chlorobenzene at a concentration of 2 wt.% and stirred for at least 1 h at 60 °C before being blended in a volume ratio of 1:1. The blended solution was stirred for at least another hour at 60 °C before use. The ca. 100 nm thick active layer was deposited via doctor blading. PEDOT:PSS (Clevios PH) from H.C. Starck was diluted in isopropyl alcohol (1:3 volume ratio) before deposition via doctor blading. The whole stack was annealed at 140 °C for 10 min on a hot plate before evaporation of a 100 nm thick Ag layer to form the top electrode. The active area of the investigated devices was 10.4 mm^2. Current density–voltage (j–V) characteristics were measured with a source measurement unit from BoTest. Illumination was provided by an Oriel Sol 1A solar simulator with AM1.5G spectra at 0.1 W/cm^2.

A UV–VIS-NIR spectrometer (Perkin Elmer – Lambda 950) was used for optical characterization of the thin films. The electrical conductivity was measured by a potentiostat (Autolab, Metrohm). Thickness of the thin films was measured by an interferometer (NanoFocus). X-ray diffraction (XRD) with CuKα radiation was done at an angle ranging from 20° to 80° by step-scanning with a step size of 0.02°.

3. Results and discussion

Table 1 compares the optical, electrical and crystalline properties of i-ZnO versus AZO. XRD spectra of AZO layers reveal a lattice stress in the 0 0 2 plane when aluminum is introduced, indicating that higher concentrations of aluminum are interstitially built into the lattice. i-ZnO particles are wurtzite type crystallites with an average crystal size of 4.2 nm while we find an average crystal size of 4.0 nm

for the converted AZO layers [24]. The optical band gap is determined by plotting $(\alpha h\nu)^2$ against $h\nu$ from UV/VIS absorption data. The optical bandgap can be found by extrapolating the linear portion of the curve to zero absorption [24]. The transmittance of the two materials is comparable. The most important difference is the increase in conductivity by about three orders of magnitude for AZO. A more detailed study of the ZnO layers will be published elsewhere [24].

Table 1
Comparison between the thin film properties of i-ZnO and AZO. The difference in the optical bandgap cannot be discussed in terms of the Moss-Burstein model due to the different synthesis, processing and conversion conditions of the i-ZnO versus the AZO film.

EIL	Crystallite size (nm)	Work function (eV)	Optical bandgap (eV)	Conductivity (S/cm)
i-ZnO	4.2	4.3	3.45	2.22×10^{-6}
AZO	4.0	4.2	3.34	2.35×10^{-3}

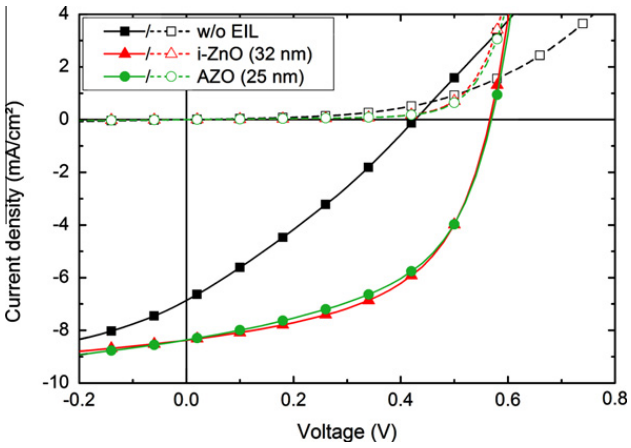

Fig. 2. j–V characteristics of solar cells without EIL, thin i-ZnO and AZO films.

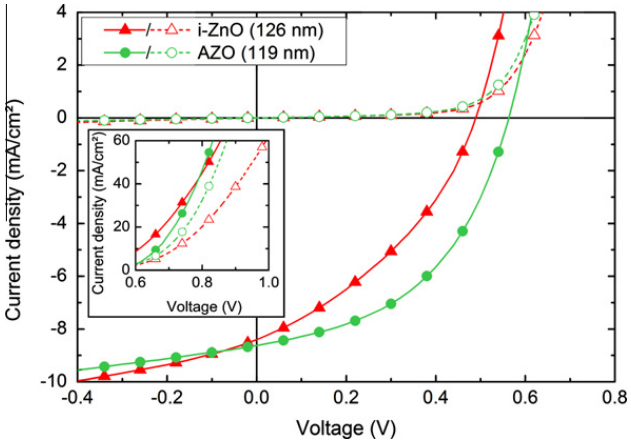

Fig. 3. j–V characteristics of solar cells with thick i-ZnO and AZO films. The inset shows the injection behavior in detail.

The layer stack of the investigated devices is shown in Fig. 1. The j–V characteristics of typical solar cells with thin i-ZnO and AZO layers (around 30 nm) are depicted in Fig. 2 and devices with thick EIL layers (above 100 nm) are shown in Fig. 3. The solar cell data for all configurations is summarized in Table 2.

A device without EIL is shown as reference in Fig. 2 as well. The j–V characteristics of the devices are dominated by a large, so-called photoshunt [25] and are further injection limited, which results in a nominal very high serial resistance of 23.6 Ω cm^2 (calculated from the slope around 1.25 V). Both loss mechanisms result from the non-selective ITO–PCBM interface. The photoshunt can be identified by the difference in slope of the illuminated versus the dark j–V curve at negative applied voltages. It originates from the several orders of magnitude higher charge carrier density of the active layer under illumination. The same mechanism is responsible for photoconductivity as well seen under forward bias as an increased injection current density. In case of the poorly charge selective ITO–PCBM interface, holes are more easily injected into the active layer at the nominal cathode. Therefore the shunt resistance scales with the conductivity of the active layer. Together with the ITO–PCBM contact resistance, this results in a decrease in the open circuit voltage (V_{OC}, 426 mV), short circuit current density (j_{SC}, −6.86 mA/cm^2), fill factor (FF, 29.2%) and consequently in a poor power conversion efficiency (PCE) of only 0.85%.

Thin layers (≈30 nm) of i-ZnO and AZO provide a much better electron selective interface and ohmic cathode contact. Losses at the cathode interface are minimized, because the electrons are extracted to i-ZnO or AZO, both at a higher work function than bare ITO. This results in increased FF, V_{OC} and j_{SC} and a significantly higher PCE of around 2.5% for both EILs. The series resistance of both device configurations is around 1.1 Ω cm^2 and well within expectations.

Increasing the layer thickness of the i-ZnO from around 30 to over 100 nm results in a severely reduced device performance from 2.5% to 1.5%. The main losses are a reduction of the FF from 53.9% to 37.7% and a reduction of the V_{OC} from 565 to 486 mV. These losses originate dominantly from three different mechanisms, which can be observed in the j–V-characteristics. First, an increase of the series resistance from 1.1 to 3.2 Ω cm^2 (see inset of Fig. 3), is

Table 2
Key parameters of the solar cells.

	V_{OC} (mV)	j_{SC} (mA/cm^2)	PCE (%)	FF (%)	R_S (Ω cm^2)	R_{Shunt} (kΩ cm^2)	$R_{Shunt/light}$ (kΩ cm^2)
w/o EIL	426	−6.86	0.85	29.2	23.6	3.0	0.29
i-ZnO (32 nm)	565	−8.41	2.56	53.9	1.1	6.2	0.59
i-ZnO (126 nm)	486	−8.40	1.54	37.7	3.2	3.1	0.33
AZO (25 nm)	569	−8.36	2.42	50.8	1.1	4.9	0.44
AZO (119 nm)	558	−8.69	2.40	49.4	1.2	3.9	0.50

caused by the thick i-ZnO layer. The higher R_S results dominantly in a FF loss. The V_{OC} loss is more subtle. The increased series resistance due to the i-ZnO layer is not expected to influence V_{OC} unless significant carrier recombination occurs in this region. Given the good charge selectivity of the ZnO layer, we exclude this loss mechanism. A contribution to the FF and V_{OC} loss originates from the already introduced photoshunt, which is much more strongly expressed in the case of thick i-ZnO layer. Photoshunts are a result of an interface-shunt, i.e. a defect shunting the electrode and the semiconductor. The photoshunt resistance is strongly dependent on the minority carrier blocking properties of the interface, the so called contact permeability of the buffer layers. This translates in our architecture to a defect, where holes become injected via the ZnO directly into the active layer [25]. We note that the photoshunt seems to emerge with increased i-ZnO layer thickness, as the shunt resistance under illumination is reduced from 0.59 kΩ cm^2 for the thin i-ZnO EIL down to 0.33 kΩ cm^2 for the thicker i-ZnO EIL (see Table 2). The dark shunt resistance also decreases from 6.0 to 3.1 kΩ cm^2. This is an indication for a reduced layer quality of the thick films. In summary, the photoshunt contributes to the losses in V_{OC} and FF. The third loss mechanism is associated with the photoconductivity of the EIL, which is much more significant for the i-ZnO based devices as compared to the AZO based devices. Illuminated i-ZnO is significantly more conductive, which leads to enhanced carrier injection under forward bias. Overall, this effect causes an increased current density under illumination (see inset of Fig. 3). This increased injected current does already compensate the photovoltaic current at lower bias, and in summary, the V_{OC} becomes reduced. This photoconductivity effect is responsible for the biggest part of the V_{OC} loss.

Solar cells with a thicker AZO EIL do not suffer from these defects. The series resistance of a device with a ~120 nm AZO layer is still as low as 1.2 Ω cm^2, which shows, that the contribution of the AZO EIL is negligible. For thicker AZO EIL the photoshunt is maintained at values larger than 0.45 kΩ cm^2, so the V_{OC} and the FF are not affected that much as for the thick i-ZnO EILs. All key parameters like FF, V_{OC}, j_{SC} and PCE remain constant for AZO layer thicknesses between 30 and 120 nm. In summary, doped ZnO opens the possibility to incorporate thick interface layers into the device architecture without sacrificing efficiency.

4. Conclusion

In this work we discussed the interface layer specifications as required from a reliable, large volume printing process for polymer solar cells. A thick electron injection layer using a solution processed aluminum-doped ZnO with high conductivity was suggested for this purpose. An increase of the intrinsic ZnO layer from 30 to ~120 nm reduced the device performance from initially 2.5% to 1.5%. The main losses are a reduction of the FF and V_{OC}, which are caused by the photoconductivity of the i-ZnO layer, the photoshunt behavior of the devices as well as its higher serial resistance. Aluminum doped ZnO could be processed as thick as 120 nm without causing losses. In the next step, the annealing temperature of the AZO films has to be reduced to around 150 °C, before these films can be processed on plastic substrates. Thick pin-hole free layers with good coverage are a prerequisite for the reliable large scale printing of organic solar cells with low shunts and high yield. In the presented concept, we incorporated thick electron injection layers into the devices. We propose that mechanically robust, thick EIL and hole injection layers (HIL) will be beneficial for the processing of thin active layers. This concept appears as an interesting strategy to optimize the lifetime and performance of single junction as well as tandem junction solar cells.

Acknowledgements

This work was funded by a German Research Foundation Project Grant (DFG; BR 4031/1-1) and the authors gratefully acknowledge the support of the Cluster of Excellence 'Engineering of Advanced Materials' at the University of Erlangen-Nuremberg, which is funded by the German Research Foundation (DFG) within the framework of its 'Excellence Initiative'. The authors would like to thank Lothar Sims, René Kogler and Jens Hauch from Konarka Technologies Inc., for the possibility to use the Kelvin Probe measurement setup.

References

[1] C.J. Brabec, N.S. Sariciftci, J.C. Hummelen, Plastic solar cells, Adv. Funct. Mater. 11 (1) (2001) 15–26.
[2] C.J. Brabec, Organic photovoltaics: technology and market, Sol. Energy Mater. Sol. Cells 83 (2–3) (2004) 273–292.
[3] S.K. Hau, H.-L. Yip, N.S. Baek, J. Zou, K. O'Malley, A.K.-Y. Jen, Air-stable inverted flexible polymer solar cells using zinc oxide nanoparticles as an electron selective layer, Appl. Phys. Lett. 92 (25) (2008) 253301–253303.
[4] C. Waldauf, M. Morana, P. Denk, P. Schilinsky, K. Coakley, S.A. Choulis, C.J. Brabec, Highly efficient inverted organic photovoltaics using solution based titanium oxide as electron selective contact, Appl. Phys. Lett. 89 (23) (2006) 233513–233517.
[5] B. Paci, A. Generosi, V.R. Albertini, P. Perfetti, R.D. Bettignies, C. Sentein, Time-resolved morphological study of organic thin film solar cells based on calcium/aluminium cathode material, Chem. Phys. Lett. 461 (1–3) (2008) 77–81.
[6] F.C. Krebs, Air stable polymer photovoltaics based on a process free from vacuum steps and fullerenes, Sol. Energy Mater. Sol. Cells 92 (7) (2008) 715–726.
[7] M. Jørgensen, K. Norrman, F.C. Krebs, Stability/degradation of polymer solar cells, Sol. Energy Mater. Sol. Cells 92 (7) (2008) 686–714.
[8] M.S. White, D.C. Olson, S.E. Shaheen, N. Kopidakis, D.S. Ginley, Inverted bulk-heterojunction organic photovoltaic device using a solution-derived ZnO underlayer, Appl. Phys. Lett. 89 (14) (2006) 143513–143517.
[9] S.K. Hau, H.-L. Yip, H. Ma, A.K.-Y. Jen, High performance ambient processed inverted polymer solar cells through interfacial modification with a fullerene self-assembled monolayer, Appl. Phys. Lett. 93 (23) (2008) 253301–253303.
[10] P. Ravirajan, A.M. Peiró, M.K. Nazeeruddin, M. Graetzel, D.D.C. Bradley, J.R. Durrant, J. Nelson, Hybrid polymer/zinc oxide photovoltaic devices with vertically oriented ZnO nanorods and an amphiphilic molecular interface layer, J. Phys. Chem. B 110 (15) (2006) 7635–7639.
[11] U. Ozgur, Y.I. Alivov, C. Liu, A. Teke, M.A. Reshchikov, S. Dogan, V. Avrutin, S.-J. Cho, H.A. Morkoc, Comprehensive review of ZnO materials and devices, J. Appl. Phys. 98 (4) (2005) 41103–41301.
[12] J. Hou, H.-Y. Chen, S. Zhang, G. Li, Y. Yang, Synthesis, characterization, and photovoltaic properties of a low band gap

polymer based on silole-containing polythiophenes and 2,1,3-benzothiadiazole, J. Am. Chem. Soc. 130 (48) (2008) 16144–16145.
[13] Y. Zou, A. Najari, P. Berrouard, S. Beaupré, B.R. Aích, Y. Tao, M.A. Leclerc, Thieno[3,4-c]pyrrole-4,6-dione-based copolymer for efficient solar cells, J. Am. Chem. Soc. 132 (15) (2010) 5330–5331.
[14] Y. Liang, Z. Xu, J. Xia, S.-T. Tsai, Y. Wu, G. Li, C. Ray, L. Yu, For the bright future – bulk heterojunction polymer solar cells with power conversion efficiency of 7.4%, Adv. Mater. 22 (20) (2010) 135–138.
[15] S.H. Park, A. Roy, S. Beaupre, S. Cho, N. Coates, J.S. Moon, D. Moses, M. Leclerc, K. Lee, A.J. Heeger, Bulk heterojunction solar cells with internal quantum efficiency approaching 100%, Nat. Photon. 3 (5) (2009) 297–302.
[16] J. Peet, J.Y. Kim, N.E. Coates, W.L. Ma, D. Moses, A.J. Heeger, G.C. Bazan, Efficiency enhancement in low-bandgap polymer solar cells by processing with alkane dithiols, Nat. Mater. 6 (7) (2007) 497–500.
[17] E. Wang, L. Wang, L. Lan, C. Luo, W. Zhuang, J. Peng, Y. Cao, High-performance polymer heterojunction solar cells of a polysilafluorene derivative, Appl. Phys. Lett. 92 (3) (2008) 33303–33307.
[18] G. Dennler, K. Forberich, T. Ameri, C. Waldauf, P. Denk, C.J. Brabec, K. Hingerl, A.J. Heeger, Design of efficient organic tandem cells: on the interplay between molecular absorption and layer sequence, J. Appl. Phys. 102 (12) (2007) 123106–123109.
[19] S. Ray, R. Das, A.K. Barua, Performance of double junction a-Si solar cells by using ZnO:Al films with different electrical and optical properties at the n/metal interface, Sol. Energy Mater. Sol. Cells 74 (1–4) (2002) 387–392.
[20] A.E. Delahoy, L. Chen, M. Akhtar, B. Sang, S. Guo, New technologies for CIGS photovoltaics, Sol. Energy 77 (6) (2004) 785–793.
[21] J. Hanisch, E. Ahlswede, M. Powalla, Contacts for semitransparent organic solar cells, EPJ Appl. Phys. 37 (3) (2007) 261–264.
[22] O. Harnack, C. Pacholski, H. Weller, A. Yasuda, J.M. Wessels, Rectifying behavior of electrically aligned ZnO nanorods, Nano Lett. 3 (8) (2003) 1097–1101.
[23] M.J. Alam, D.C. Cameron, Preparation and properties of transparent conductive aluminum-doped zinc oxide thin films by sol–gel process, J. Vac. Sci. Technol. (2001) 1642–1646.
[24] H. Oh, J. Krantz, I. Litzov, T. Stubhan, L. Pinna, C.J. Brabec, Comparison of various sol–gel derived metal oxide layers for inverted organic solar cells, Sol. Energy Mater. Sol. Cells 95 (8) (2011) 2194–2199.
[25] C. Waldauf, M.C. Scharber, P. Schilinsky, J.A. Hauch, C.J. Brabec, Physics of organic bulk heterojunction devices for photovoltaic applications, J. Appl. Phys. 99 (10) (2006) 104503–104506.